Chapter 3
Pre-treatment of Waste Copper Dust (I): Potential of Oxidative Roasting–Density Separation–Sulphuric Acid Leaching Technology for Copper Recovery

Daniel Ogochukwu Okanigbe, Abimbola Patricia Popoola, and Abraham Adewale Adeleke

3.1 Introduction

Numerous researchers have thoroughly investigated and reported on the treatment of waste copper dust (WCD) [1–11]. These procedures, which include roasting WCD [12, 13], smelting WCD [14–16], roasting WCD followed by dissolution [17–20], and sulphuric acid leaching of WCD [21–23], have been presented or used at various levels (pilot and/or industrial levels).

In comparison with hydrochloric (HCl) and nitric acid (HNO_3), sulphuric acid (H_2SO_4) is the most effective and popular acid for leaching oxides, according to Teir et al. [24], Trans et al. [25], and Habashi [26]. In order to recover the copper value present in waste/by-products containing copper, such as WCD, sulphuric acid has been employed extensively [11, 27].

In WCD, copper is primarily present as copper oxides and, to a lesser extent, as copper sulphides [5]. Yes, it is noticeable given that 70,000–100,000 kilograms of WCD is produced annually [2, 3, 28]. Chalcopyrite forms passive layers over itself

D. O. Okanigbe (✉)
Department of Chemical Metallurgical and Materials Engineering, Faculty of Engineering and the Built Environment, Tshwane University of Technology, Pretoria, South Africa

Pantheon Virtual Engineering Solutions, Nigel, South Africa
e-mail: okanigbedo@tut.ac.za; okanigbeogochukwu@gmail.com

A. P. Popoola
Department of Chemical, Metallurgical and Materials Engineering, Faculty of Engineering and the Built Environment, Tshwane University of Technology, Pretoria, South Africa

A. A. Adeleke
Department of Materials Science and Engineering, Faculty of Technology, Obafemi Awolowo University, Ile-ife, Osun state, Nigeria

D. O. Okanigbe, A. P. Popoola (eds.), *Resource Recovery and Recycling from Waste Metal Dust*, https://doi.org/10.1007/978-3-031-22492-8_3

during sulphuric acid leaching, which slows the rate of dissolution and ultimately results in low copper recovery, therefore recovering its copper sulphides like chalcopyrite with this method will defeat the purpose of conserving mineral resources [29, 30]. However, a pre-treatment method frequently preferred in the industry for copper sulphides [17–20] involves subjecting the WCD to either low temperatures (partial roasting) [31] or high temperatures (dead roasting) [32] in the hope of producing dissolvable oxidative products (or calcines) for copper recovery.

In addition, the complex mineralogy (mineralogy that might contain gangue minerals such clays, jarosites, gypsum, quartz, and micas) and porosity structure of WCD continue to produce side reactions [33] and poor mass transfer of solution. Sulphuric acid consumption from side effects is a problem and thus reduces the effectiveness of leaching. The diffusion mechanism in the solid particles of the WCD can also have an impact on the leaching efficiency; this mechanism is dependent on the pore distribution (also known as porosity) of the WCD and can have a positive or negative impact on the leaching efficiency depending on the nature of the pore distribution in the WCD, which in turn affects the mass transfer of solution to the sites of leaching reactions.

In light of the foregoing, research into the impact of pre-treatments including oxidative roasting and density separation of WCD on mineralogy, side reactions, and mass transfer of solution is required to determine whether copper recovery may be improved. The results of these investigations will thus be presented in this chapter.

3.2 Experimental Method

3.2.1 Material

Waste Metal Dust

The WCD from South Africa was used as source of metal ore for this study.

3.2.2 Methods

3.2.2.1 Pre-Treatment Methods

Oxidative Roasting

Read Okanigbe, Popoola and Adeleke [7], Okanigbe et al. [9], and Okanigbe [34] for further information on thermal behaviour, thermodynamic modelling, experiment design, and the experimental process of oxidative roasting pre-treatment of the WCD.

Density Separation Method

The articles by Okanigbe et al. [8], Okanigbe [34], and Okanigbe et al. [35] provide more information on sample preparation, density determination, experiment design, and the experimental process of density separation pre-treatment of WCD.

3.3 Results and Discussion

3.3.1 Effect of Pre-Treatments on Mineralogy of WCD

3.3.1.1 Oxidative Roasting

Figure 3.1a, b displays the differential scanning calorimetry (DSC) and thermogravimetric analyser (TGA) results at various heating rates. The DSC curves have similar shapes, but when the heating rate rises, the peaks alter at higher temperatures (Fig. 3.1a). It was discovered that heating the WCD between 40 °C and 138 °C causes moisture to evaporate, which on the TGA curve equates to a loss of mass as well (Fig. 3.1b). Between 120 °C and 150 °C, an endothermic peak was seen in the DSC profile; this was most likely caused by the loss of water during crystallization, which occurs in species of minerals like gypsum [7]. However, pyrite began to oxidize at intervals of 173 °C–261 °C, which was shown by mass loss in the TGA curve (Fig. 3.1b) and an exothermic peak at 248 °C in the DSC profile (Fig. 3.1a).

The publication by Okanigbe, Popoola, and Adeleke [5] contains the findings of the XRD analysis of the heat treated WCD.

Thermodynamic modelling of the oxidative roasting of WCD (using FACTSage 6.8 version) was done utilizing the results of the DSC (Fig. 3.1a), TGA (Fig. 3.1b), and XRD analyses (Table 3.1).

Based on these modelled results, a special superimposed predominant area diagram (SPAD) was created for the Cu-S-O and Fe-S-O systems (also known as Cu-Fe-S-O) at temperatures of 100 °C, 680 °C, 740 °C, and 800 °C (Fig. 3.2a, b).

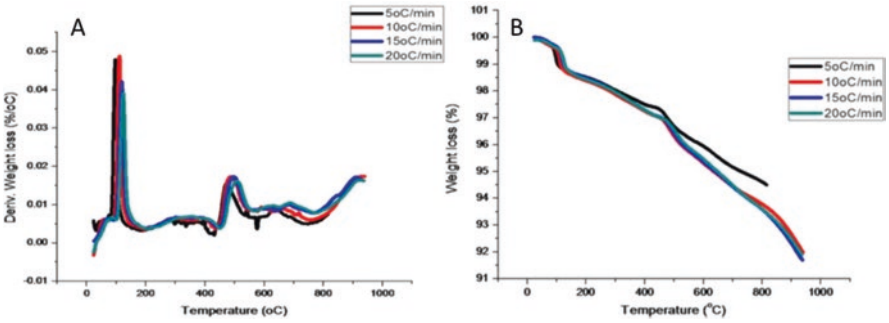

Fig. 3.1 Thermal Behaviour of CSD as derived from (**a**) DSC and (**b**) TGA Curves at 5, 10, 15, and 20 °C/Min [7]

Table 3.1 Mineralogical Composition and Specific Gravity of WCD [5, 6]

No.	Minerals	Chemical Formulae	Content (Wt %)	Specific gravity
1	Cuprospinel	$Cu_{0.98}O_{1.02}$	24.34	6.50 (Landes [36])
2	Chalcopyrite	$Cu_{6.88}Fe_{4.00}S_{8.00}$	7.95	4.20 (Landes [36])
3	Mullite	$Al(Al_{0.69}Si_{1.22}O_{4.85})$	42.97	3.16 (Tripathi et al. [37])
4	Gypsum	$Ca(SO_{4.00})(H_{2.00}O)_{2.00}$	11.69	2.33 (Landes [36])
5	Quartz	$SiO_{2.00}$	11.45	2.70 (Landes [36])
6	Magnetite	$Fe_{2.96}O_{4.00}$	1.60	4.95 (Landes [36])

The SPAD model displays the Cu-Fe-S-O system's potential phases at low temperature (680 °C), intermediate temperature (740 °C), and high temperature (800 °C) (Fig. 3.2a, b).

Copper and iron sulphides, such as chalcopyrite and bornite (Fig. 3.2a) and pyrite (Fig. 3.2b), respectively, oxidize at lower temperatures to form sulphates and oxysulphates, such as chalcocyanite and dolerophanite. These minerals transform into oxides like tenorite, hematite, and magnetite at high temperatures (800 °C). Accordingly, it will be anticipated to detect copper ferrite/Cuprospinel-$CuFe_2O_4$, which was created in the WCD at temperatures of 900 °C, which is near to the operating temperature (i.e. oxidative roasting in reverberatory furnace-1400 °C) under which it was produced (Fig. 3.2a). This modelled premise fits in nicely with a prior report on the characteristics of this specific WCD [5].

According to theory, chalcopyrite native solid-phase migration into spinel form ferrite is what creates cuprospinel [7]. $CuSO_4$, Fe_3O_4, CuO, and Fe_2O_3 are intermediary phases that allow $CuFe_2O_4$ to form inside grains. The thermodynamic model was also used to predict the theoretical equilibrium composition (TEC) of the WCD after roasting in the air (Eq. 3.1).

$$\begin{aligned}&24.34\left(Cu_2O\right)\left(Fe_2O_3\right)+7.95CuFeS_2+42.97Al_6Si_2O_{13}+11.69CaSO_4\left(H_2O\right)_2\\&+11.45SiO_2+1.60MgFe_2O_4+\left(71\%N_2,19\%O_2,10\%CO_2\right)Air\end{aligned} \tag{3.1}$$

The thermodynamic model for WCD was experimentally validated by roasting the WCD in a muffle furnace with the furnace door slightly ajar to let in fresh air. It was found that even at 800 °C, the mullite, quartz, and gypsum in the WCD as it was received persisted in the roast product unaltered (Fig. 3.3). While gypsum was observed to lose its water of crystallization at temperatures between 120 °C and 200 °C to form anhydrite (Fig. 3.3), this was not the case for iron in WCD, which oxidized into iron II (Fe^{2+}) and/or iron III (Fe^{3+}). These findings are consistent with those made from analyses of DSC and TGA results (Fig. 3.1a, b).

Because some sulphur did not completely oxidize during partial roasting, sulphur is still present in the roast products (RP) as Cu_2S and FeS. In the RP, oxygen coexists with either copper or iron. It was found that varying temperature and time were related to variations in the sulphate and oxide levels in the RP. Certain circumstances made it more likely to produce sulphates than oxides, and vice versa (Fig. 3.4).

In terms of mineralogical composition, it was found that test 8 with treatment settings of 800 °C for 2 hrs produced the closest experimental result to TEC [9].

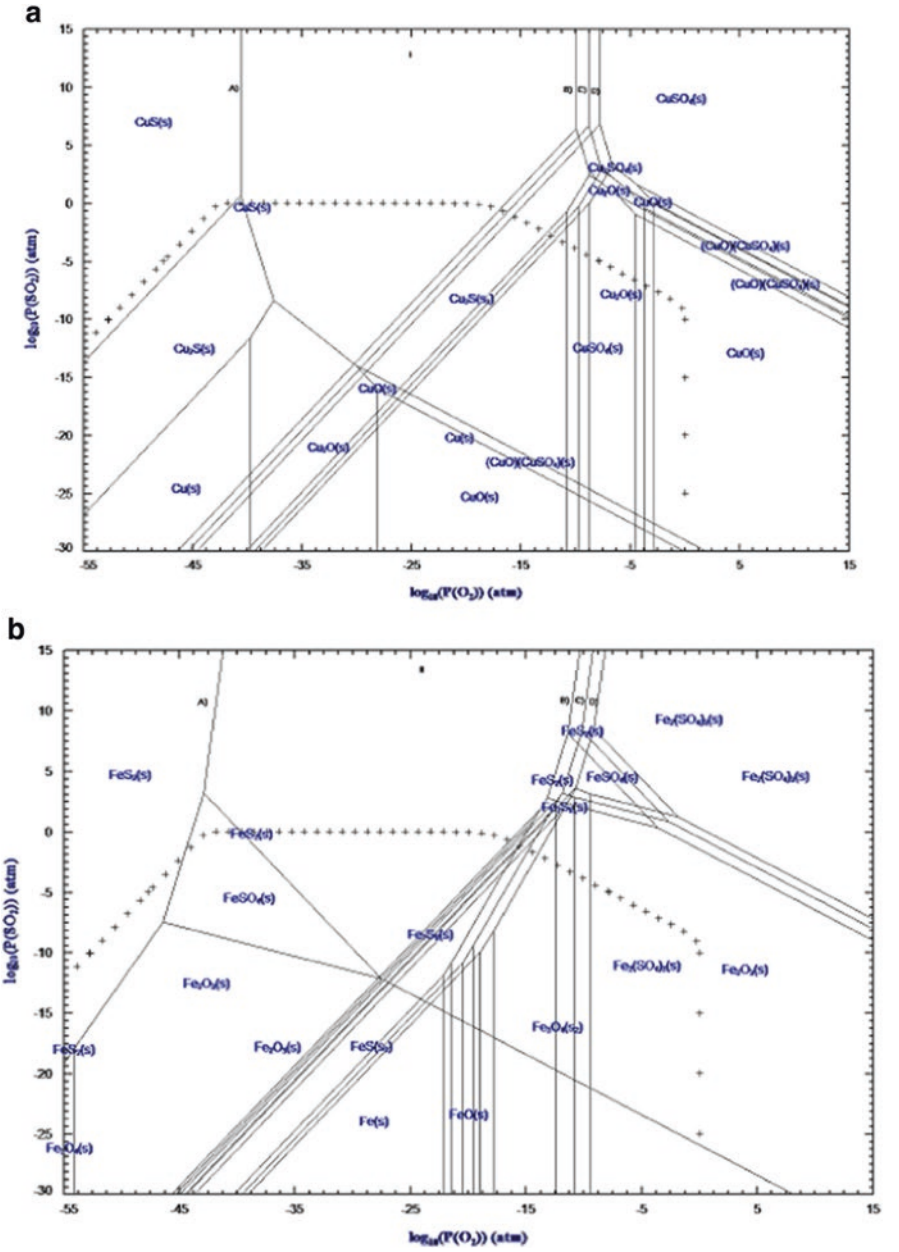

Fig. 3.2 Superimposed predominance area (**a**) Cu-S-O and (**b**) Fe-S-O system diagrams at 100 °C, 680 °C, 740 °C, and 800 °C [7]

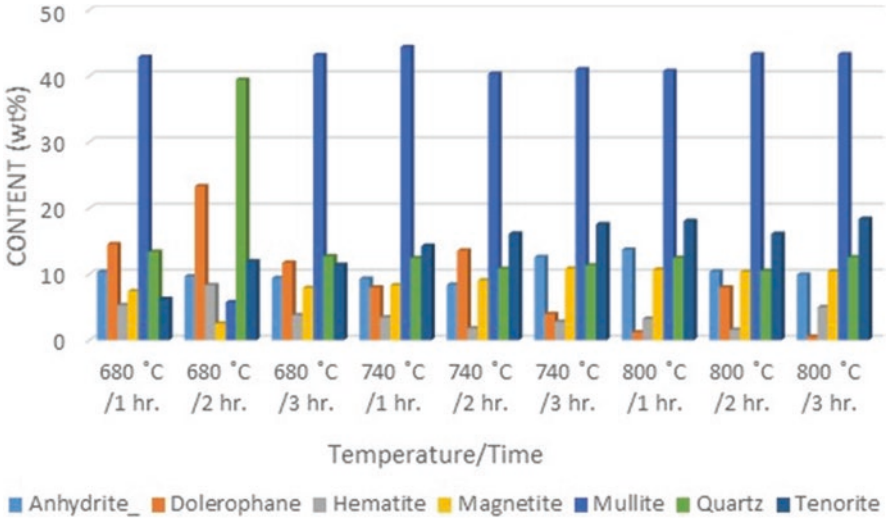

Fig. 3.3 XRD Result of the Oxidative Roasting Carried Out on WCD

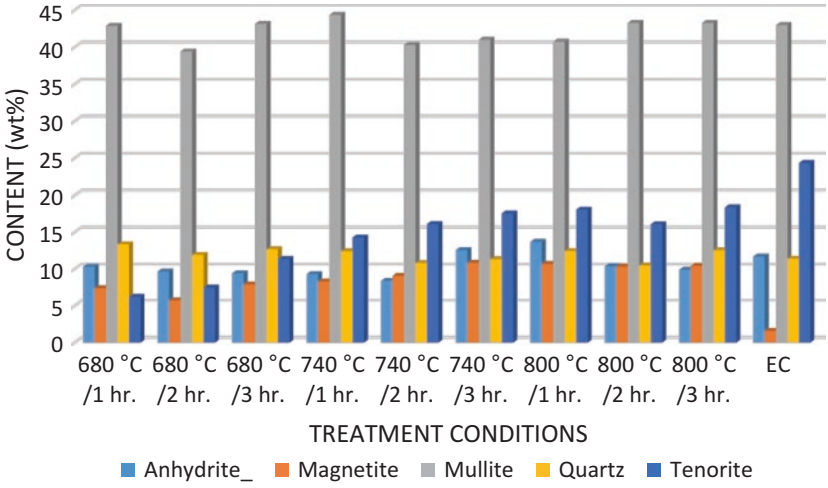

Fig. 3.4 Experimental Equilibrium Compositions at Different Test Conditions

3.3.1.2 Density Separation

In Table 3.2, you can see the mineralogical composition of copper value in tailings obtained from TC-7 of DS. According to Table 3.1 and Fig. 3.5, the composition of the copper value in this group of tailings is primarily composed of copper sulfides with a minor quantity of metallic copper, which is consistent with the theoretical deductions previously established. The copper value that reported to the tailings is primarily made up of sulfides with a very tiny proportion of metallic copper, i.e. according to the mineralogical analysis of the tailings acquired after DS (Table 3.2).

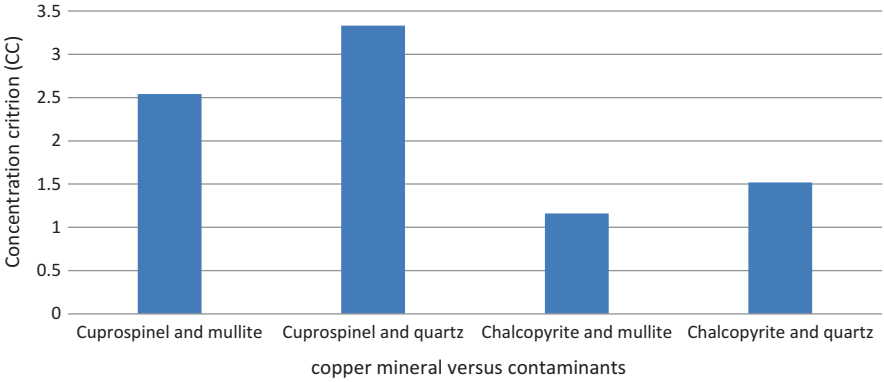

Fig. 3.5 Concentration criterion for different minerals in the WCD

Table 3.2 Mineralogical Composition of Copper Value in Tailings from TC-7 of DS

No	Minerals	Chemical formulae of minerals	CC (between CuS and SiO_2/ SiO_2-Al_2O_3)
1	Copper	$Cu_{4.00}$	≤2.5
2	Chalcopyrite	$Cu_{4.00}$ $Fe_{4.00}$ $S_{8.00}$	≤ 2.5
3	Pyrite	$Fe_{4.00}$ $S_{8.00}$	≤2.5
4	Wassonite	$Cu_{28.00}$ $S_{16.00}$	≤2.5
5	Tochilinite	$Fe_{8.00}$ $S_{10.00}$	≤2.5
6	Isocubanite	$Cu_{1.33}$ $Fe_{2.67}$ $S_{4.00}$	≤2.5

Despite being less in content than copper oxides (Table 3.1), these copper sulfides are nevertheless of significant value, especially in light of the 70,000–100,000 kilograms of WCD produced annually [2, 3, 28]. Therefore, it is advised that oxidative roasting (400–500 °C) be combined with DS in the pre-treatment protocol to change these copper sulfides into copper sulphates or oxides before physical separation.

3.3.1.3 Effect of Pre-Treatment on Classification of WCD

The transformation (i.e. phase change) of minerals (Fig. 3.3) was the major outcome of using oxidative roasting alone to pre-treat WCD. The objective of minimizing adverse effects (i.e. side reactions and poor porosity structures) while copper is being leached from the WCD persist. Since the gangue minerals (such as mullite, gypsum, and quartz), which cause the side reactions during leaching, are still tightly linked to copper value.

Copper oxide, iron oxide, calcium oxide, and magnesium oxide were much more prevalent in the concentrates than in the tailings, hereafter referred to as group A, after the physical separation of WCD with the centrifugal concentrator. However, the tailings had substantially more silicon oxide, aluminium oxide, and titanium

oxide than concentrate did (Fig. 3.6). The optimal combination of maximal copper content and minimal quartz and mullite content, which acts as a baseline for centrifugal performance, was found in Test 7, and it was also noted (Fig. 3.7).

The information acquired (Figs. 3.8, 3.9, 3.10, 3.11, 3.12, 3.13, 3.14, and 3.15) shows that the separation of copper oxide minerals from undesirable minerals

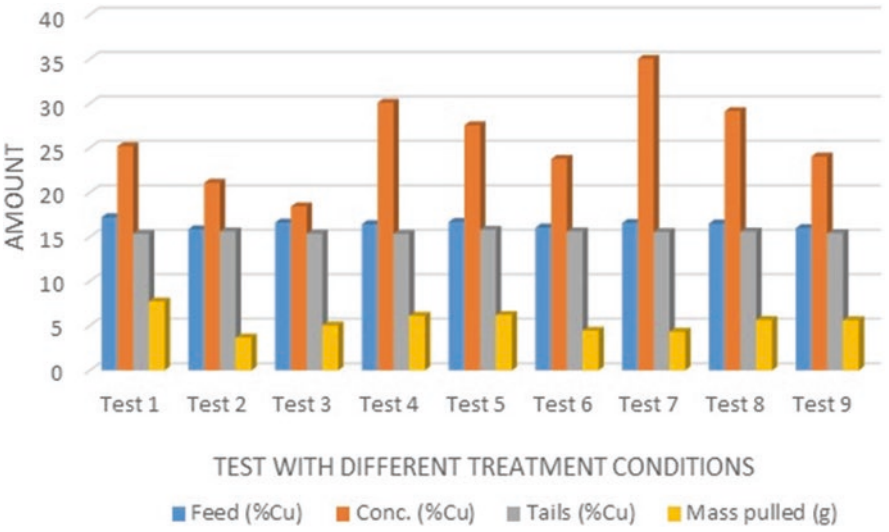

Fig. 3.6 Total Mass Pull for Tests Performed with the KGC

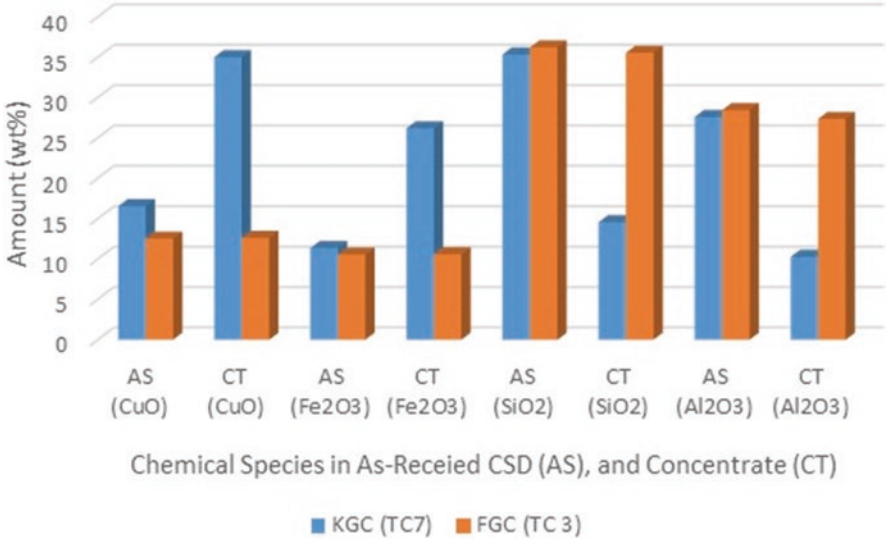

Fig. 3.7 Total Mass Pull for Tests Carried out with the KGC

(aluminium oxide and silicon oxide) was made possible by applying this pre-treatment method (i.e. DS) alone. With this outcome, side reactions during the leaching of copper from the WCD can be brought to the barest minimal (Okanigbe et al. [8]).

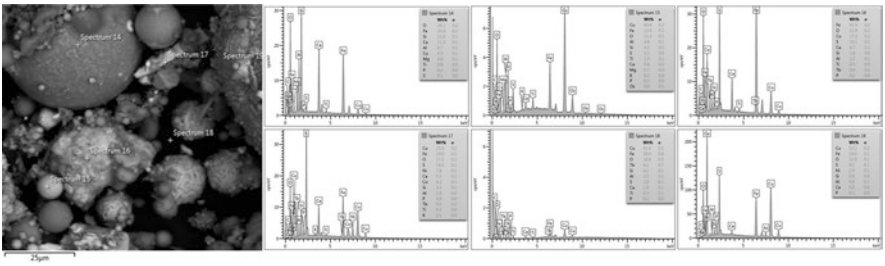

Fig. 3.8 Spectrums showing copper, aluminium, and silicon contents in concentrate from DS test 1

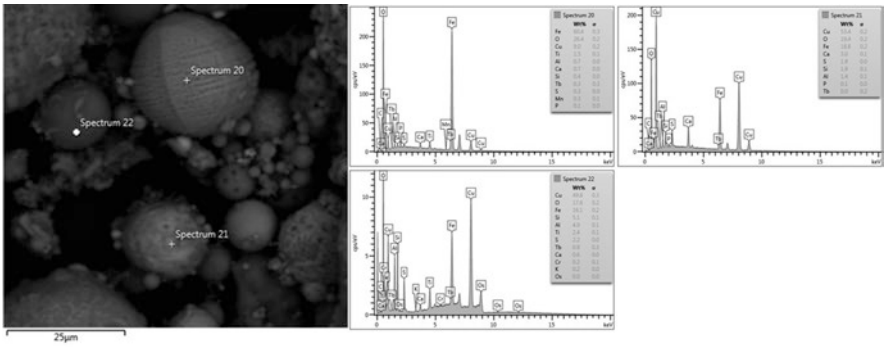

Fig. 3.9 Spectrums showing copper, aluminium, and silicon contents in concentrate from DS test 2

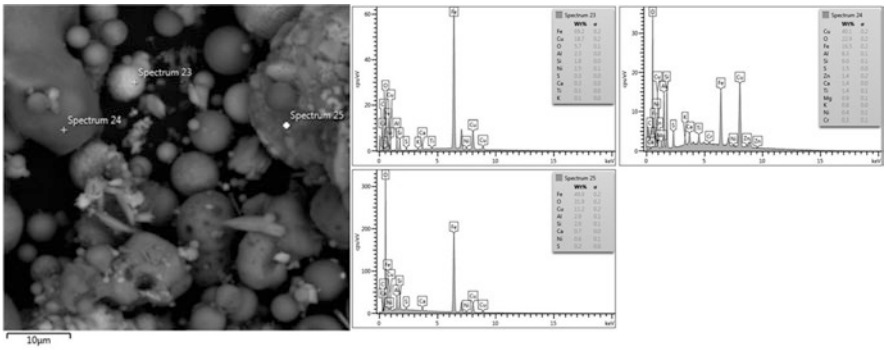

Fig. 3.10 Spectrums showing copper, aluminium, and silicon contents in concentrate from DS test 3

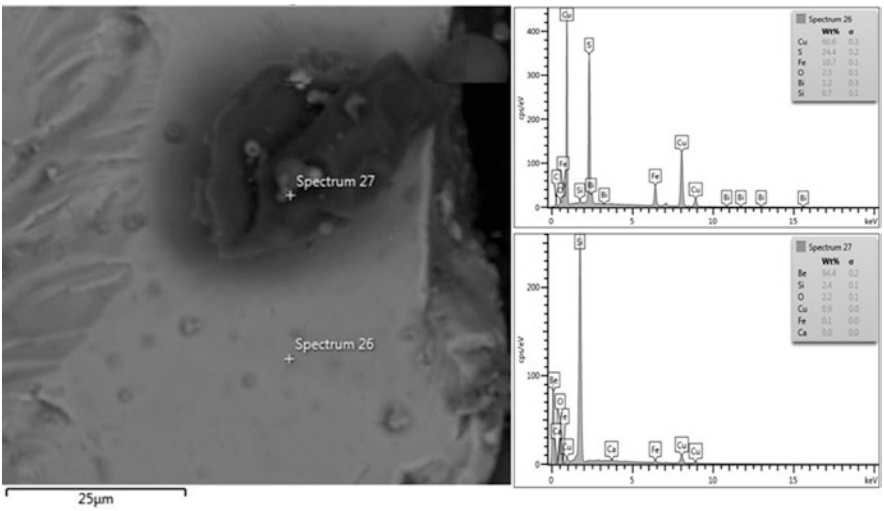

Fig. 3.11 Spectrums showing copper, aluminium, and silicon contents in concentrate from DS test 4

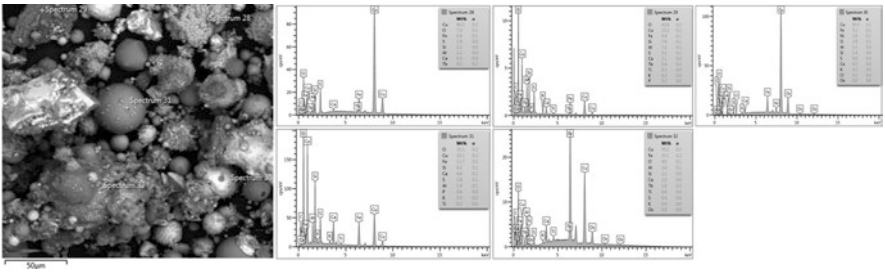

Fig. 3.12 Spectrums showing copper, aluminium, and silicon contents in concentrate from DS test 5

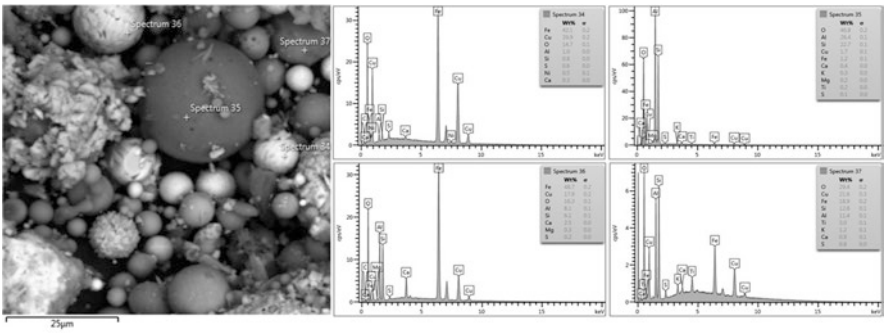

Fig. 3.13 Spectrums showing copper, aluminium, and silicon contents in concentrate from DS test 6

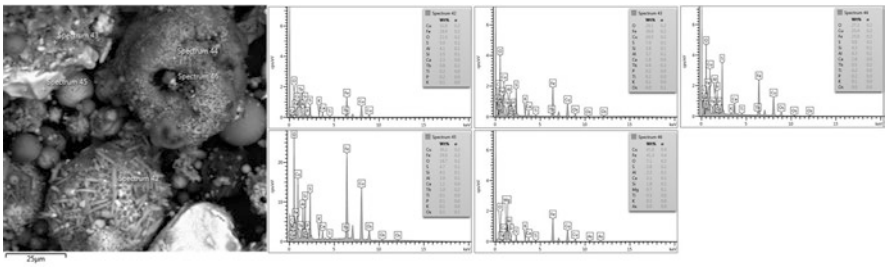

Fig. 3.14 Spectrums showing copper, aluminium, and silicon contents in concentrate from DS test 8

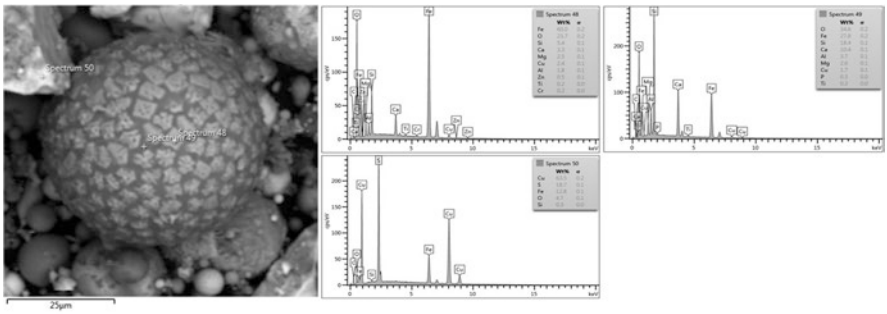

Fig. 3.15 Spectrums showing copper, aluminium, and silicon contents in concentrate from DS test 9

3.3.1.4 Effect of Pre-Treatment on Micro-Porosities

The force that attempts to pull an object in a circle toward its centre is known as centripetal force.

Centripetal force is occasionally experienced by objects, although not as frequently as gravitational force or frictional force. Only when moving in a circle can you experience centripetal force. It makes it possible for items to move along a circular path without being forced off the path by inertia. The condition in which we rotate, swing any object, or travel in orbits around a centre is an excellent example. We talk about the centripetal force in relation to the classification of the WCD in this section of Chap. 4. The force necessary for circular motion is the centripetal force, and in accordance with Herivel's [38] interpretation of Newton's second law of motion, net force equals mass times acceleration. The centripetal acceleration is the acceleration in a homogeneous circular motion. Thus, using Eq. 3.2, it is possible to calculate the centripetal force's (F) magnitude. As a result, Eq. 3.2 can be used to estimate the size of the centripetal force acting on WCD particles during classification.

$$C = MA \tag{3.2}$$

where

C = centripetal force; M = mass of solid used for test; A = acceleration due to gravity

Hence:

$$C = 83.0562\,\text{g} \times 9.8\frac{\text{m}}{\text{s}^2}$$

$$C = 813.9508\,\text{gm}/\text{s}^2$$

$$C = 813.9508\,\text{N}$$

However, it is possible to estimate the centripetal force that really affected the particles during WCD classification as follows:

For level 1 (i.e. 60 G)

$$C = 60 \times 813.9508\,\text{N}$$

$$C = 48{,}837.048\,\text{N}$$

This force (48,837.048 N) is comparable to what 86 adults of average weight would apply to a single particle (Fig. 3.16).

For level 2 (i.e. 90 G)

$$\text{C} = 90 \times 813.9508\,\text{N}$$

$$\text{C} = 73{,}255.572\,\text{N}$$

This force (73, 255.572 N) is comparable to what 129 adults of average weight would apply to a single particle (Fig. 3.17).

For level 3 (i.e. 120 G)

$$\text{C} = 120 \times 813.9508\,\text{N}$$

$$\text{C} = 97{,}674.096\,\text{N}$$

This centripetal force, which is equal to 97,674.096 N, is comparable to what 172 adults of average weight would apply to a single particle (Fig. 3.18).

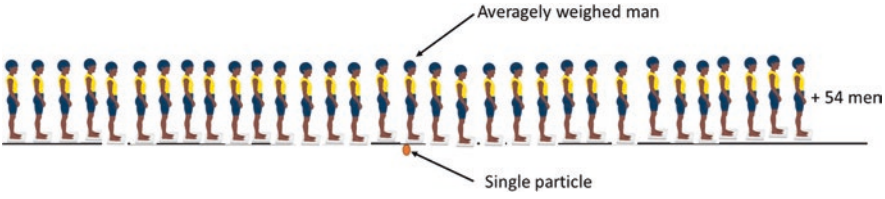

Fig. 3.16 Illustration of the force applied to a single particle by 86 averagely weighed men

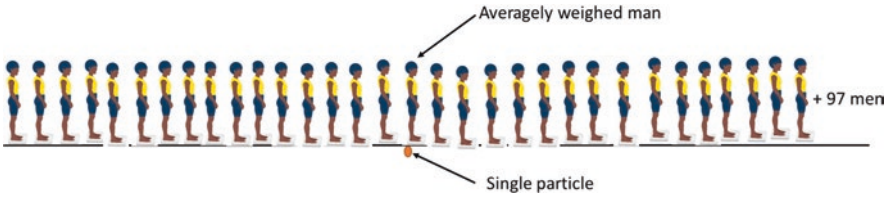

Fig. 3.17 Illustration of the force applied to a particle by 129 adults of average weight

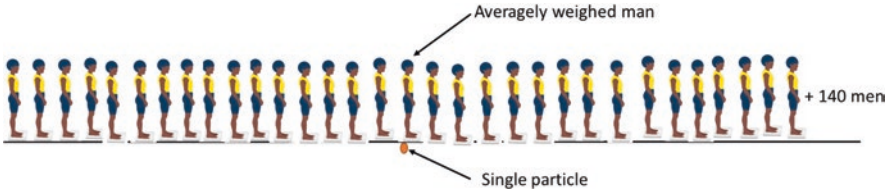

Fig. 3.18 Picture showing the force applied to a single particle by 172 adults of average weight

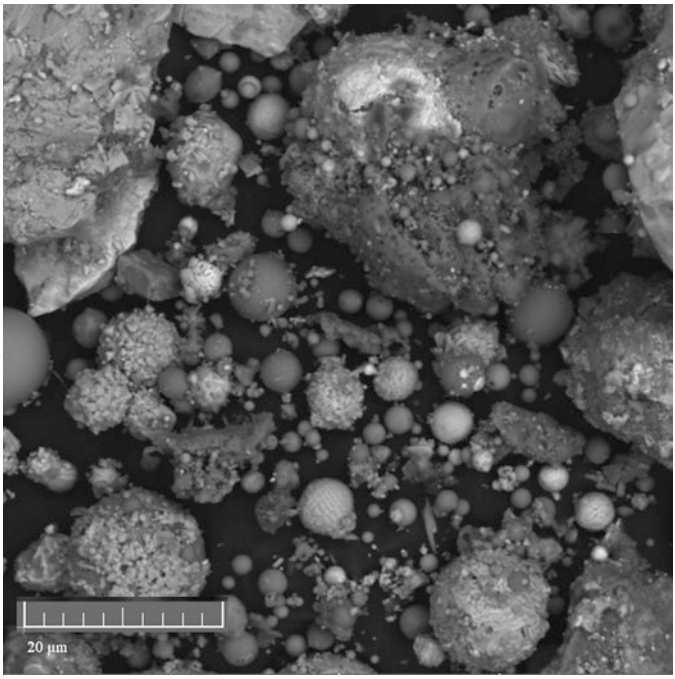

Fig. 3.19 SEM photo of Concentrate from DS Test 1

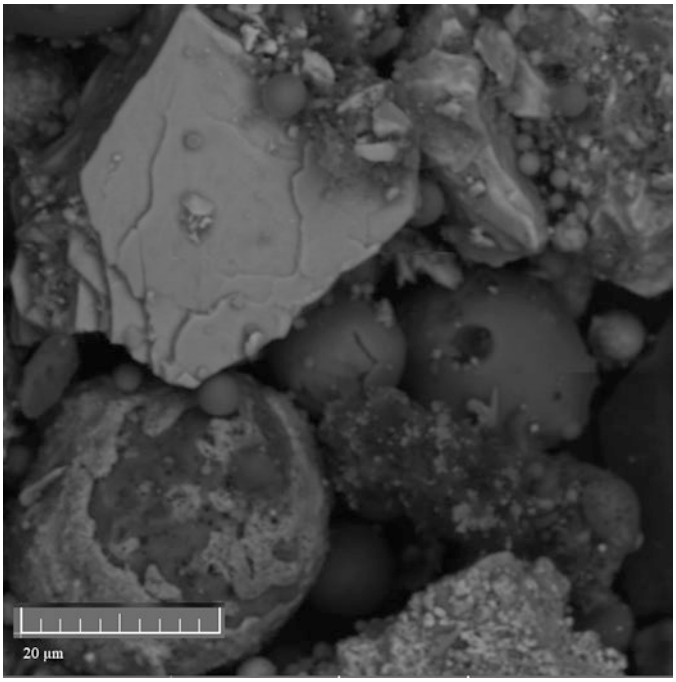

Fig. 3.20 SEM photo of Concentrate from DS Test 2

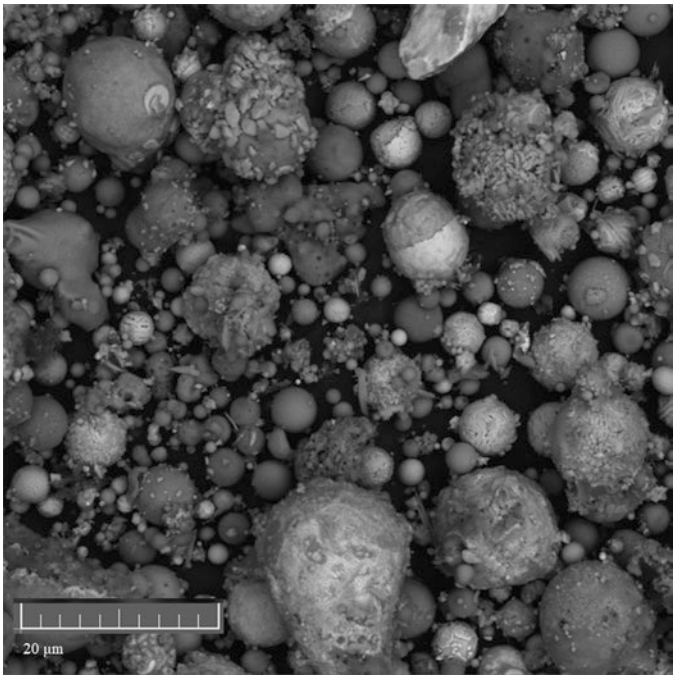

Fig. 3.21 SEM photo of Concentrate from DS Test 3

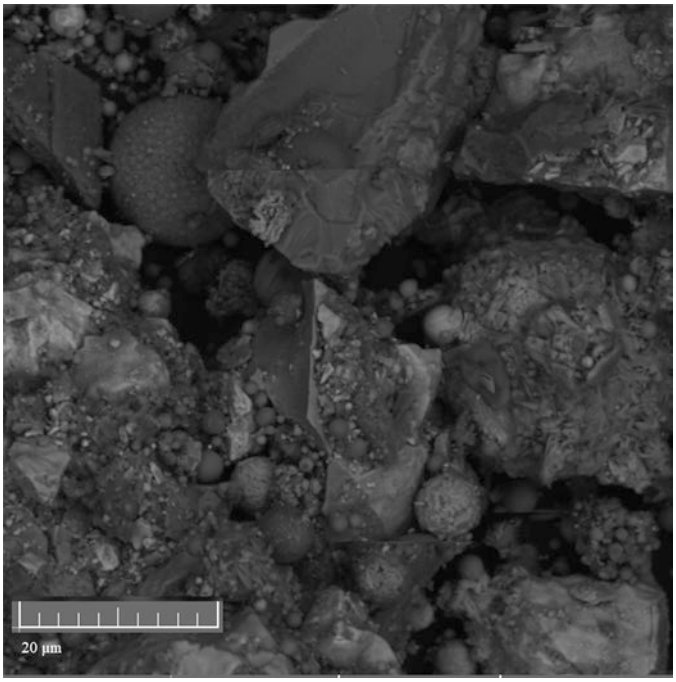

Fig. 3.22 SEM photo of Concentrate from DS Test 4

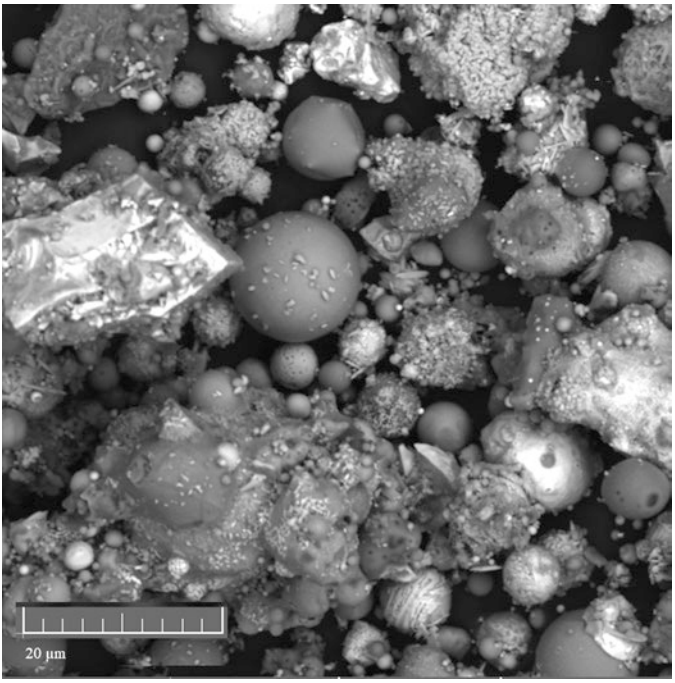

Fig. 3.23 SEM photo of Concentrate from DS Test 5

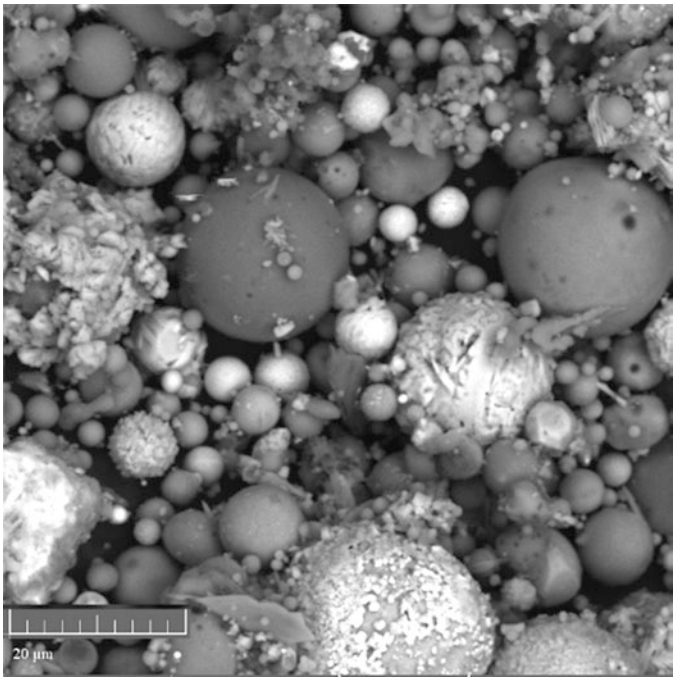

Fig. 3.24 SEM photo of Concentrate from DS Test 6

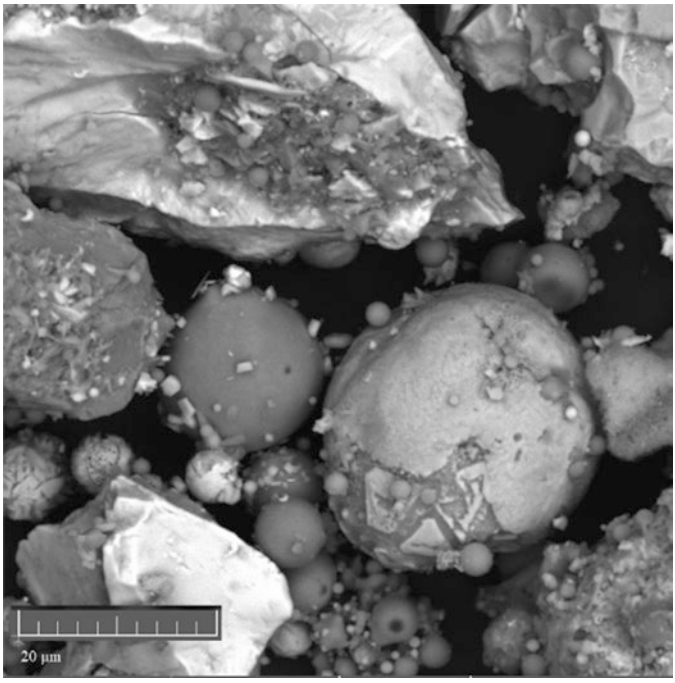

Fig. 3.25 SEM photo of Concentrate from DS Test 7

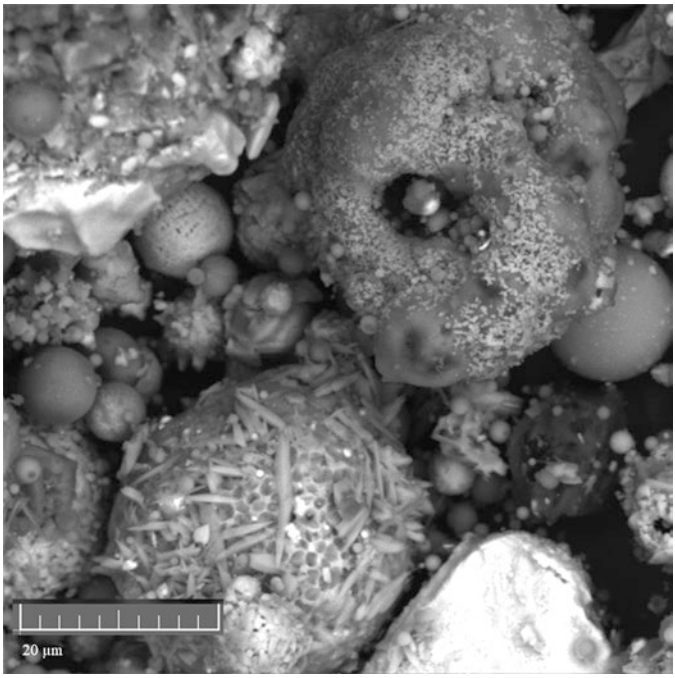

Fig. 3.26 SEM photo of Concentrate from DS Test 8

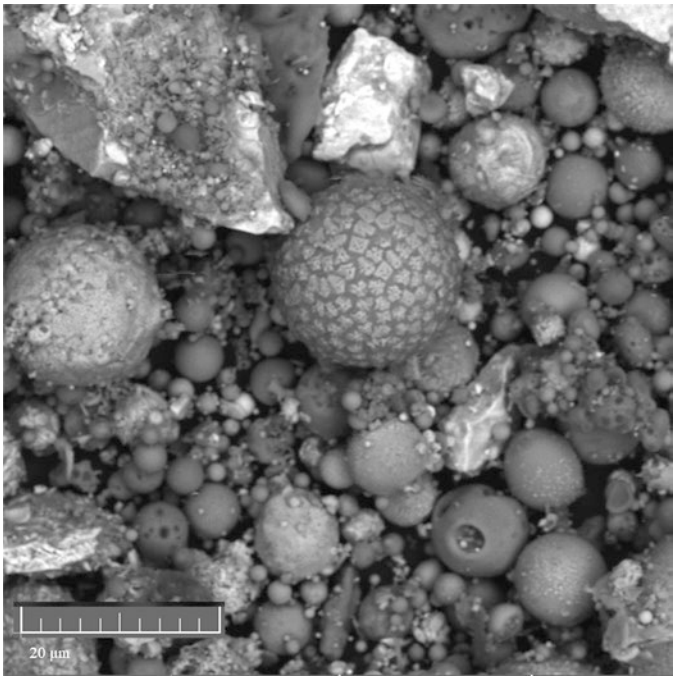

Fig. 3.27 SEM photo of Concentrate from DS Test 9

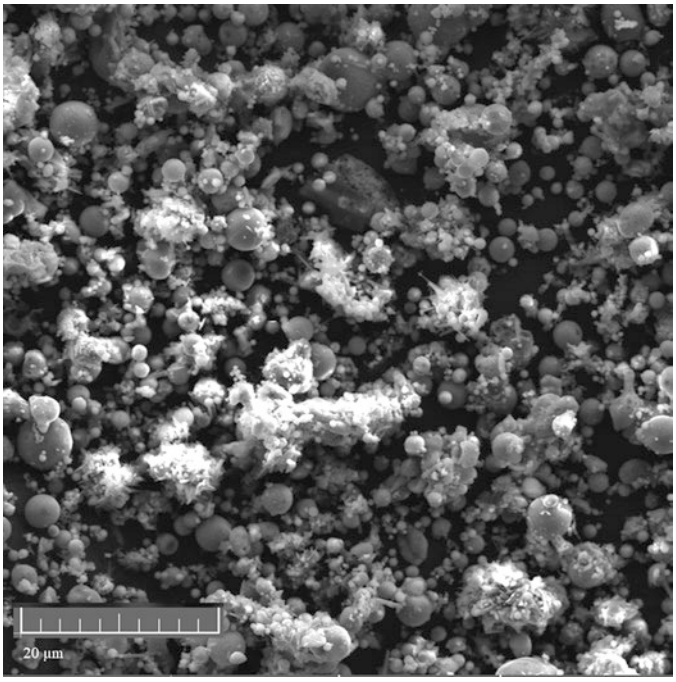

Fig. 3.28 SEM photo of As-received WCD

Consequently, the concentrates after classification exhibit micro-porosities such as cracks and peels as illustrated by SEM images in Figs. 3.19, 3.20, 3.21, 3.22, 3.23, 3.24, 3.25, 3.26, and 3.27 when compared to the as-received WCD (Fig. 3.28).

The concentrate from Test 7 yielded the greatest copper content, which was measured (Fig. 3.25). On the basis of the SEM photos that follow, it can be seen that the number of smaller particles gradually decreased until the ideal condition (test 7) was attained, which displayed the fewest number of smaller particles. This finding is consistent with the prior EDS results in this chapter (Figs. 3.8, 3.9, 3.10, 3.11, 3.12, 3.13, 3.14, and 3.15).

3.3.1.5 Effect of Pre-Treatment on Surface Area, Pore Volume, and Pore Diameter of CSD

Both the pore volume (0.0087 to 0.0027 cm^3/g) and BET surface area (4.1730 to 0.4634 m^2/g) for RP significantly decreased. Shrinkage due to moisture loss caused particle aggregation, sintering, and formation of larger-sized pores (i.e. 82.9530 Å and 233.5759 Å for AS and RP, respectively) in RP (Table 3.3). Although CT had a much bigger pore diameter (increase from 82.9530 Å in CSD to 410.8530 Å in concentrate), it had a much lower specific surface area (down from 4.1730 m^2/g in the WCD to 0.3321 m^2/g in concentrate). In this case, the change was attributed to

Table 3.3 BET Measurement of WCD [34]

BET	WCD	RP	Difference	CT	Difference
Surface area (m^2/g)	4.166100 4.179900	0.458100 0.468700	– –	0.320500 0.343700	– –
Average	4.173000	0.463400	−900%	0.332100	−1200%
Pore volume (cm^3/g)	0.008506 0.008802	0.002663 0.002749	– –	0.003139 0.003685	– –
Average	0.008654	0.002706	−320%	0.003412	−200%
Pore diameter (Å)	80.057900 85.848100	213.654300 253.497500	– –	396.514200 425.191800	– –
Average	82.953000	233.575900	+280%	410.853000	+400%

the CT having more heavier/larger particles and less lighter/smaller particles. The leaching rate of copper from this WCD is anticipated to benefit from the increased pore diameter (Table 3.3).

3.4 Conclusions

The aim of this chapter is to present the potentials of introducing DS into OR-SAL technology. This was achieved by comparing OR and DS pre-treatments. Result showed average surface area of WCD decreased by 900% and 1200% when pre-treated with OR and DS, respectively. The pore volume decreased by 320% and 200% when WCD was pre-treated using OR and DS, respectively. However, pore diameter increased by 280% and 400% when WCD was pre-treated with OR and DS, respectively. Furthermore, DS pre-treated particles revealed enhanced micro-porosities in form of peels and cracks. Significant amounts of gangue minerals (e.g. aluminium and silicon) reported to the tailings, presupposing reduced SR and enhanced PS. In conclusion, OR-DS-SAL is a technology with capacity to enhance copper recovery from WCD. Hence, recommended.

Acknowledgements The author will want to appreciate Tshwane University of Technology, Pretoria, South Africa, for facilities made available.

References

1. A.A. Adeleke, A.P.I. Popoola, O.M. Popoola, D.O. Okanigbe, Experimentation, modeling, and optimum conditions of pyro-hydrometallurgical-precipitation reaction technology for recovery of copper as oxide of nanoparticles from a copper dust, in *Energy Technology 2020: Recycling, Carbon Dioxide Management, and Other Technologies*, (Springer, Cham, 2020), pp. 189–201
2. E. Balladares, U. Kelm, S. Helle, R. Parra, E. Araneda, Chemical-mineralogical characterization of copper smelting flue dust. Dyna **81**(186), 11–18 (2014)

3. T.K. Ha, B.H. Kwon, K.S. Park, D. Mohapatra, Selective leaching and recovery of bismuth as Bi_2O_3 from copper smelter converter dust. Sep. Purif. Technol. **142**, 116–122 (2015)
4. A. Morales, M. Cruells, A. Roca, R. Bergó, Treatment of copper flash smelter flue dusts for copper and zinc extraction and arsenic stabilization. Hydrometallurgy **105**(1–2), 148–154 (2010)
5. D.O. Okanigbe, A.P.I. Popoola, A.A. Adeleke, Characterization of copper smelter dust for copper recovery. Proc. Manuf **7**, 121–126 (2017)
6. D.O. Okanigbe, A.P.I. Popoola, A.A. Adeleke, Hydrometallurgical processing of copper smelter dust for copper recovery as nano-particles: A review. Energ. Technol. **2017**, 205–226 (2017)
7. D.O. Okanigbe, A.P.I. Popoola, A.A. Adeleke, Thermal analysis and kinetics of the oxidative roasting process of a copper smelter dust. Int. J. Adv. Manuf. Technol. **94**(5), 2393–2400 (2018)
8. D. Okanigbe, P. Olawale, A. Popoola, A. Abraham, A. Michael, K. Andrei, Centrifugal separation experimentation and optimum predictive model development for copper recovery from waste copper smelter dust. Cogent Eng **5**(1), 1551175 (2018)
9. D.O. Okanigbe, M.K. Ayomoh, O.M. Popoola, P.A. Popoola, V.S. Aigbodion, Oxidative roasting experimentation and optimum predictive model development for copper and iron recovery from a copper smelter dust. Results Eng **7**, 100125 (2020)
10. M. Vítková, V. Ettler, J. Hyks, T. Astrup, B. Kříbek, Leaching of metals from copper smelter flue dust (Mufulira, Zambian Copperbelt). Appl. Geochem. **26**, S263–S266 (2011)
11. J.Y. Wu, F.C. Chang, H.P. Wang, M.J. Tsai, C.H. Ko, C.C. Chen, Selective leaching process for the recovery of copper and zinc oxide from copper-containing dust. Environ. Technol. **36**(23), 2952–2958 (2015)
12. M. Carter, E.R. Vance, L.P. Aldridge, M. Zaw, G. Khoe, Immobilization of arsenic trioxide in cementitious materials, in *Australasian Institute of Mining and Metallurgy*, (1994), pp. 275–280
13. Y. Fu, L. Jiang, D. Wang, Removal of arsenic from copper smelter flue dust by calcinations. Yelian Bufen **6**, 14–16 (2000)
14. V.I. Ermakov, Complex treatment of fine dusts of Urals copper-smelting firms. Tsvetn. Met. (12), 26–30 (1979)
15. Z. Yu, Process for bismuth recovery from the flue dust of copper smelting. Huaxue Shijie **28**(10), 465–468 (1987)
16. H. Mochida, O. Iida, Copper smelter flue dust treatment (Kokai Tokkyo Koho, Jap, 1988), p. 3
17. Sumitomo Metal Mining, Metal Recovery from Flue Dust Containing Copper. Japan Patent 57.201.577 (1982)
18. Z.B. Yin, E. Caba, L. Barron, D. Belin, W. Morris, M. Vosika, R. Bartlett, Copper extraction from smelter flue dust by lime-roast/ammoniacal heap leaching, in *Residues and Effluents: Processing and Environmental Considerations*, (1992), pp. 255–267
19. C.T. Mulale, M.D. Mwema, G.B. Mashala, Retreatment of dust waste from the copper smelter and converter, in *Global Symposium on Recycling and Clean Technology*, vol. 2, (1999), pp. 1201–1208
20. B. Gorai, R.K. Jana, Z.H. Khan, Electrorefining electrolyte from copper plant dust. Mater. Trans. **43**(3), 532–536 (2002)
21. R. Hanks et al., "Bismuth at Rokana Copper Smelter, Zambia: Its Behavior and Extraction from Flue Dusts," Trans. IMM, 88 (1979), pp. C99–C106.
22. M.P. Smirnov, V.T. Khvan, G.A. Bibenina, R.P. Kefilyan, N.I. Il'yasov, Complex treatment of lead and rhenium containing sulfate dusts from copper plants. Tsvetnye Metally **6**, 3–6 (1984)
23. Z.W. Zhang, W. Lu, F. Zheng, Separation and recovery of copper and zinc from flue dust. Huanjing Kexue **11**(6), 1012–1016 (1992)
24. S. Teir, H. Revitzer, S. Eloneva, C.J. Fogelholm, R. Zevenhoven, Dissolution of natural serpentinite in mineral and organic acids. Int. J. Miner. Process. **83**(1–2), 36–46 (2007)
25. L.H. Tran, K.K. Mueller, L. Coudert, J.F. Blais, Optimized indium solubilization from LCD panels using H2SO4 leaching. Waste Manag. **114**, 53–61 (2020)

26. F. Habashi, *Metals from Ores: An Introduction to Extractive Metallurgy* (Métallurgie Extractive Québec, Sainte Foy, 2003)
27. R.K.K. Mbaya, M.M. Ramakokovhu, C.K. Thubakgale, Atmospheric pressure leaching application for the recovery of copper and nickel from low-grade sources, in *The Southern African Institute of Mining and Metallurgy (Base Metals Conference 2013)*, (The Southern African Institute of Mining and Metallurgy, Johannesburg, 2013), pp. 255–268
28. L. Qiang, I.S. Pinto, Z. Youcai, Sequential stepwise recovery of selected metals from flue dusts of secondary copper smelting. J. Clean. Prod. **84**, 663–670 (2014)
29. F. Barriga, I. Palencia, F. Carranza, The passivation of chalcopyrite subjected to ferric sulfate leaching and its reactivation with metal sulfides. Hydrometallurgy **19**, 159–167 (1987)
30. C. Klauber, A critical review of the surface chemistry of acidic ferric sulphate dissolution of chalcopyrite with regards to hindered dissolution. Int. J. Miner. Process. **86**, 1–17 (2008)
31. S.E. Khalafalla, I.D. Shah, Oxidative roasting of covellite with minimal retardation from the $CuO \cdot CuSO_4$ film. Metallur. Trans **1**(8), 2151–2156 (1970)
32. F. Magagula, High temperature roasting of sulphide concentrate and its effect on the type of precipitate formed (Doctoral dissertation, Doctoral dissertation) (2012)
33. E. Hsu, K. Barmak, A.C. West, A.H.A. Park, Advancements in the treatment and processing of electronic waste with sustainability: A review of metal extraction and recovery technologies. Green Chem. **21**(5), 919–936 (2019)
34. D.O. Okanigbe, Production of copper and copper oxide nano-particles from leach solution of low grade copper smelter dust (2019)
35. D.O. Okanigbe, A.P.I. Popoola, A.A. Adeleke, O.M. Popoola, Upgrading the copper value in a waste copper smelter dust with the falcon gravity concentrator, in *TMS Annual Meeting & Exhibition*, (Springer, Cham, 2018), pp. 283–295
36. K.K. Landes, A mineral specific gravity chart. Am. Miner. J. Earth Planet. Mater **15**(11), 534–535 (1930)
37. H.S. Tripathi, S.K. Das, B. Mukherjee, A. Ghosh, Sintered mullite from aluminous ore for refractory application. Am. Ceram. Soc. Bull. **86**(5), 9301–9306 (2007)
38. J.W. Herivel, Newton's discovery of the Law of Centrifugal Force. Isis **51**(4), 546–553 (1960)